Coarsening and Pearling Instabilities in Silver Nanofractal Aggregates

A. Lando, N. Kébaïli, Ph. Cahuzac, A. Masson, and C. Bréchignac

Laboratoire Aimé Cotton, CNRS UPR 3321, Bâtiment 505, University Paris-Sud, Campus d'Orsay, F-91405 Orsay Cedex, France

(Received 24 December 2004; revised manuscript received 12 April 2006; published 25 September 2006)

We investigate the morphological changes of 3D supported fractal aggregates generated through the deposition of silver clusters on graphite. The fractal relaxation, activated after their formation by perturbing them either by thermal annealing or by using a surfactant, as oxide molecules, carried by silver clusters in a subsequent deposition, shows evidence of two distinct fragmentation patterns. The post coarsening, driven by thermal heating, gives a broad asymmetrical distribution of fragments in agreement with a random process, whereas the entire silver fractal pearling fragmentation is driven by chemical adjunction of the surfactant.

DOI: 10.1103/PhysRevLett.97.133402 PACS numbers: 36.40.Sx, 47.20.Dr, 61.43.Hv, 81.16.−c

The construction of systems with nonequilibrium morphologies that mimic the spontaneous pattern formation in nature plays an important role in scientific disciplines as diverse as physics, chemistry, materials science, and biology [1,2]. It has been shown since the pioneering work of Mullins and Sekerka that a growing spherical nucleus becomes unstable as its radius exceeds few times a critical value [3]. Such instability may usually lead to dendritically growth giving rise to nonequilibrium morphologies with a large surface to volume ratio. After their growth these far from equilibrium systems begin to relax into more stable shapes by decreasing the overall surface area. However, if the growth processes have been extensively studied and almost understood, the relaxation after the growth is still an open question.

The theoretical studies on the instability, due to capillary forces, of nonequilibrium shapes started with the work of Rayleigh on the break of a viscous cylinder into a row of equal-sized and equal-spaced spheres [4]. His model has been recently applied to interpret the transformation of silicon [5] and copper [6] nanowires, with diameter below 50 nm, into nanospheres after thermal annealing at temperatures much below the melting point of the corresponding bulk. It has been also recently shown that the instability of fractal islands, generated through the deposition of a narrow size distribution of silver clusters with trace amounts of oxide species, follows this class of fragmentation behavior [7]. The entire fragmentation of the fractal island in small drops almost equally spaced along the fractal skeleton is governed by the ratio of the length to the width of the fractal arms [7]. This result contrasts with those obtained under thermal annealing of 2D fractals, where the coarsening of their arms is the dominant mechanism for their shape relaxation [8,9]. In this last case, the initially highly branched fingering pattern becomes smoother and the fractal evolves into a more compact shape [8] or at least broadens its arms, keeping constant its global size [9]. Two-dimensional theoretical models based on surface self-diffusion mechanism have been developed [10–12]. The main result is the loss of fingering pattern at small distance associated to a conserved frozen fractal structure at large distance [13]. Although very little concerns the fractal fragmentation, it has been calculated that if the 2D fractal is large enough a post coarsening fragmentation may occur and the fractal should evolve into an ''ensemble of circular disks with arbitrary radii in a stable equilibrium'' [14].

It may be remarked that these two different behavior patterns of shape evolution, i.e., coarsening and Rayleigh-type fragmentation, are both driven by an enhancement of the mobility of surface atoms. Up to now, these two types of behaviors have been observed individually for different systems under different conditions. Moreover, the late post-fragmentation stage following the coarsening has not been observed so far. Then it is of fundamental interest to investigate a given nonequilibrium system, which can evolve under these two behaviors, up to the late stage of its relaxation.

We have conducted this study. The experiments deal with the evolution of morphological changes of supported 3D fractal islands, generated through the deposition of a narrow size distribution of silver clusters on graphite substrate at room temperature. These clusters diffuse along the surface and aggregate to ramified structures like those observed in [Figs. 1(a) and 1(d)]. We enhanced the surface-atom mobility along the fractal arms after the formation of the fractal islands either by thermal annealing of the sample or by using a surfactant, as oxide molecules, carried by silver clusters in a subsequent deposition. As a matter of fact, it has been shown that Ag-island ripening is enhanced by Ag_2O molecules [15–17]. Our experiments provide evidence of two distinct fragmentation patterns. For thermal annealing fractal coarsens and evolves into an ensemble of drops with a large dispersion in size. On the contrary, when the primary fractal is submitted to a ''shower'' of clusters containing chemical impurities very little broadening of the fractal arms is observed. The fragmentation leads to a narrow size distribution of drops equally spaced along the fractal skeleton, in agreement with a ''Rayleigh-like'' fragmentation behavior. The dif-

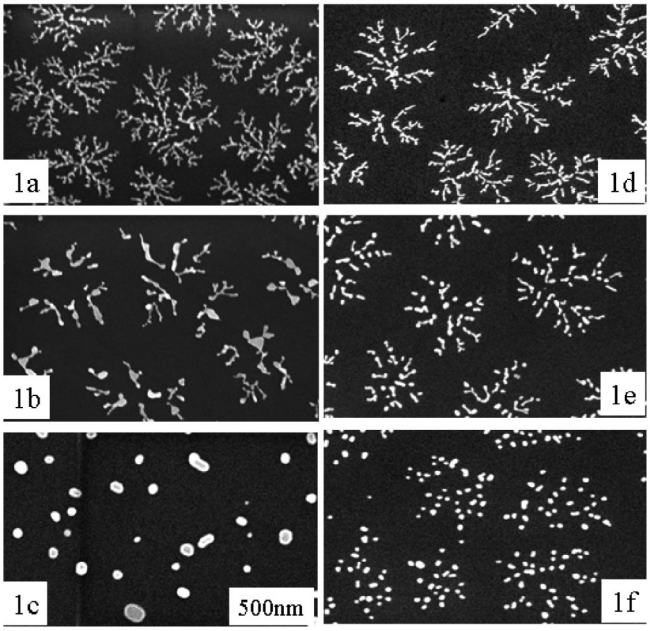

FIG. 1. SEM images showing the difference of relaxation for fractal islands undergoing either heating (left column) or chemical impurity (right column). The upper rows correspond to initial fractal islands before perturbation. The middle row shows images resulting either from the annealing during 1 h at 200 °C (b) or from subsequent deposition of clusters carrying 0.2% of oxygen (e). The lower row results either from the annealing during 1 h at 300 °C (c) or from subsequent deposition of clusters carrying 0.5% of oxygen (f).

ference in the final patterns should find their interpretation at the atomic level. Upon thermal annealing the less coordinated atoms are activated to move to a more coordinated site that promotes the smoothening, whereas chemical impurities strongly enhance the silver atom mobility around the oxygen atoms evenly distributed along the fractal arms.

In our experiments gas-phase neutral silver clusters, produced by a gas-aggregation cluster source, are deposited at low impact energy (0.05 eV/atom), on a room temperature cleaved graphite surface maintained at high vacuum (10^{-9} torr) [18]. The neutral-cluster distribution is measured using a time-of-flight mass spectrometer. A crystal quartz microbalance measures the intensity of the incident neutral cluster beam. The deposition time, from 4 to 10 minutes, is chosen depending on the cluster beam flux and the desired coverage. In our experiments fluxes of the order of 10^{10} clusters/cm^2 s were used. Since per atom kinetic energy of the incident clusters is very low compared with the binding energy (1.2 eV) of the silver clusters, fragmentation of the incident cluster is unlikely and the clusters migrate on the surface as a whole and grow into silver ramified islands. In a first set of experiments, the prepared samples are transferred under high vacuum to a chamber where they are fixed on a heating support. Annealing of the samples is performed in vacuum in a temperature range: 180 °C–400 °C, during a lapse of time that is varied from 5 to 120 minutes. After cooling, the samples were either transferred into high vacuum and imaged with a noncontact atomic force microscope (AFM), or transferred in air and imaged in a scanning electron microscope (SEM). The similarity between the images obtained from the two microscopies shows that the transfer in air does not affect the island morphologies, within our experimental time window. In a second set of experiments, the samples are prepared through successive depositions. On a graphite substrate, two different coverages were obtained by carrying out the deposition of pure silver clusters, and subsequently blocking part of the substrate by a mask and continuing the deposition of silver clusters carrying trace amounts of oxygen onto the unmasked part for an additional interval of few minutes. The oxidized clusters were obtained by adding a small amount (0.2%–1%) of oxygen to the helium gas during the cluster formation. The prepared samples are analyzed with the same techniques as aforementioned. The beauty of this method is the possibility of comparing on the same sample the influence of chemical impurity carried by clusters in subsequent depositions. We have done numerous of measurements of fractal morphological changes at various annealing times for a given temperature, and at various temperatures for a given annealing time, as well as for various impurity concentrations for chemically induced relaxation. Figure 1 displays typical examples of SEM images of multi-island fractal films obtained through deposition of pure silver clusters with a mean diameter of 3 nm [Figs. 1(a) and 1(d)], and their evolution either after annealing [Figs. 1(b) and 1(c)] or after subsequent deposition of clusters carrying impurity [Figs. 1(e) and 1(f)]. It is clear that in both cases the fractal island fragment and their fragments evolve to compact shapes, but the size distribution of the fragments as well as their organization on the substrate are quite different.

From SEM images of unperturbed fractal islands we determined the three parameters, which characterize the projection of such ramified island on the substrate: (i) the upper cutoff L, corresponding to the extended size of the island, measured by the diameter of the smallest circle enclosing the island, (ii) the lower cutoff l_0, corresponding to the width of the fractal branches, (iii) the fractal dimension D_f [19]. The asymptotic mass fractal dimension, measured for large L by using the power law relation between the mass M and L, is $D_f = 1.7 \pm 0.1$ in agreement with a diffusion limited aggregation mechanism on a surface [19]. We determine l_0 using the relation $S/P = l_0/2$ where S is the area and P the perimeter of the fractal island. This relation is obtained from the box-counting method [14]. The histograms for l_0 related to the samples presented in Fig. 1(a) and 1(d), are shown in Fig. 2(a) and 2(d). The samples resulting either from annealing in vacuum during 1 h at 200 °C [Fig. 1(b)] or from subsequent deposition of clusters carrying oxygen, when 0.2% of O_2 is

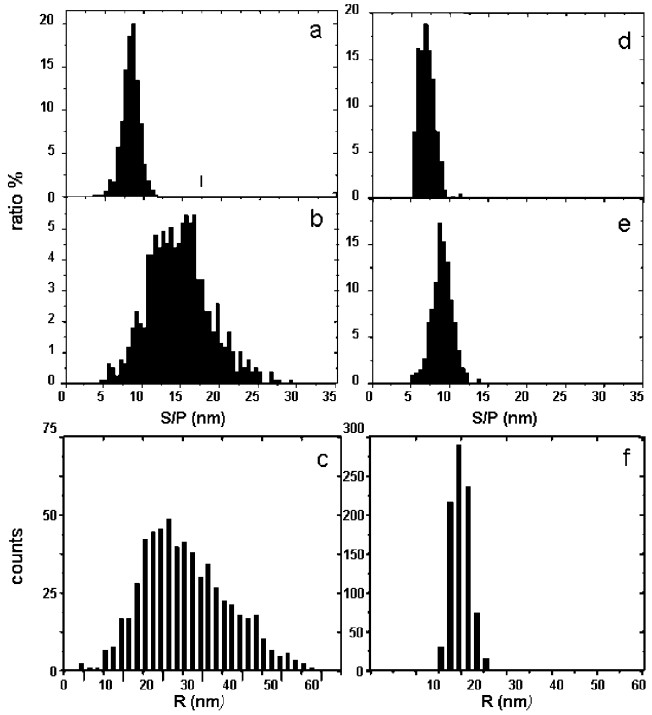

FIG. 2. Histograms of the ratio S/P measured from SEM images. The upper row is related to unperturbed fractals. The medium row depicts S/P for each fragment of a fractal island after perturbation either by annealing (b) or by adjunction of oxide molecules carried by silver clusters in a subsequent deposition (e). Lower row: histograms of the radii of the fragments measured from SEM images similar to the one shown in Fig. 1(c) and 1(f).

added to the carried gas [Fig. 1(e)] show fragmented islands with the reminiscence of fractal shapes indicating that in both cases the large structure, i.e., the upper cutoff L, remain frozen. Such a behavior of morphological change, keeping constant the upper cutoff of the object, is a signature of shape modification through surface-atom diffusion mechanism, where the volume diffusion is prohibited [12,14]. The resulting histograms of the fractal branch widths are given in Fig. 2(b) and 2(e). Figure 2(b) shows a clear broadening of the branches ($l_0/2$ peaks at 15 nm) accompanied with a large disparity in width in agreement with a coarsening mechanism [11]. On the contrary, Fig. 2(e) shows a narrow branch-width distribution, where only a very small broadening is observed ($l_0/2$ peaks at 9 nm). At the ultimate stage of the process, we observe that the number of fragments through addition of surfactant is about 1 order of magnitude larger than through annealing. In Fig. 1(f) the relaxed fragments are distributed along the fractal skeleton, whereas in Fig. 1(c) the too large polydispersity of the fragment sizes make difficult the reminiscence of the initial islands. Figure 2, lower row, displays the corresponding histograms of the mean radius of each fragment measured from SEM images. In the case of thermal annealing relaxation [Fig. 1(c)], the histogram of the fragment radii [Fig. 2(c)] is very broad exhibiting a asymmetrical envelope that may be assimilated with a lognormal curve characteristic of a stochastic mechanism. Evidence of small fragments with sizes smaller than the initial branch-width is seen. On the contrary, in the case of relaxation following adjunction of chemical impurity [Fig. 1(f)], the histogram [Fig. 2(f)] presents a narrow symmetrical distribution that can be fitted by a Gaussian profile peaking at $R = 19.2$ nm with half width at half maximum of 2.5 nm.

We focus now on the first steps of the processes. Two observables have been considered: the time evolution of the branch width and the autocorrelation function of the nearest neighbor distance. From our annealing measurements performed at 180 °C during a given time t varying from 3 to 120 mn, we measured the broadening of the fractal arm width l from S/P [Fig. 3(left)]. After a latent period, we found at long time the scaling law $l \approx l_0 t^{0.20\pm0.01}$, that is similar to the time evolution observed for the coarsening of radially grown fractal viscous fingering patterns due to surface tension [9]. Our observation is also consistent with the Monte Carlo calculations of Irisawa *et al.* [11], on the thermal relaxation of diffusion limited aggregation (DLA)-2D fractal aggregates under edge-atom diffusion. Moreover, their calculations show that the smoothing of the local roughness of the fractal branches occurs via local edge-atom diffusion, which jumps from less coordinated sites towards more coordinated ones. On the contrary, the shape change following the deposition of clusters carrying chemical impurities does not present coarsening mechanism.

The nearest-neighbor distance λ between fragments is given by the autocorrelation function. For the annealing case, no oscillating function is found, in agreement with a random fragmentation process. In the case of fragmentation through addition of surfactant, we determined this function for numerous of impurity concentrations. Figure 3 (right) shows an example of such a function with maxima separated by $\lambda = 70$ nm. For all the samples considered, the average value is $\langle\lambda\rangle = 73$ nm $\pm$ 10 nm. As a consequence, the ratio between the average spacing $\langle\lambda\rangle$ and the initial diameter $l_0 = 16$ nm $\pm$ 2 nm of the fractal branch prior to its fragmentation is well defined and is

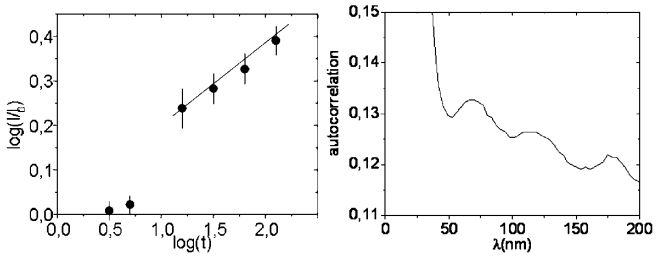

FIG. 3. Left panel: Evolution of the branch ratio l/l_0 as a function of the annealing time t; l_0 is the width before annealing. Right panel: autocorrelation function for chemically induced relaxation; the first maximum deals with fragments belonging to the same initial fractal branch.

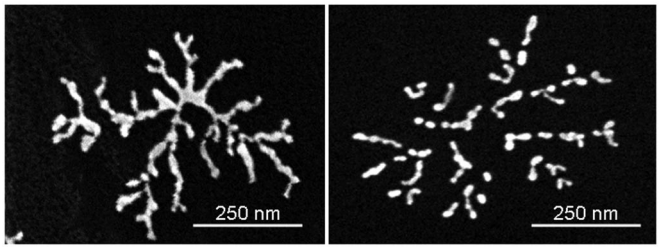

FIG. 4. SEM images comparing the early stage of the fractal shape evolution by using either annealing (left) or chemical activation (right). Notice the drastic broadening for annealing, whereas for chemical activation the pearling structure is already present without significant broadening.

4.6 ± 1.2. This value is curiously in agreement with the Rayleigh's criterion for the drop formation in a inviscid liquid column [4]. However, no calculations at the atomic level are yet available for this mechanism.

At this stage it is interesting to compare the fractal island relaxation for thermal annealing with the relaxation by adding surfactant, at the early stage of the process when fragmentation starts. Figure 4 shows a detailed comparison between a fractal structure annealed during 15 mn at 180 °C, and a similar structure submitted to a subsequent shower of clusters carrying a low concentration of impurities. For the thermal fragmentation, primary fragments of coarsened fractal branches exhibit smoothed shapes, whereas in the chemically induced relaxation, evidence of pearled shapes of fractal branches is seen. In this latter case, it must be remarked that even at this early stage, the measured periodicity is already $\langle\lambda\rangle$. The discrimination between the two distinct fragmentation paths is already present. These two possible routes, even though the basic process, i.e., the surface-silver atom enhanced mobility, is common, can be explained as follows. Upon annealing, the mobility of all the silver atoms is activated. However, the probability to diffuse is linked to the number of bonds to be broken. Surface atoms are less coordinated than volume atoms. They are the most likely to diffuse to a strongly coordinated site. This leads first to the decrease of the local roughness (coarsening), and second to necks formation which are statistically distributed along the fractal arms. The structure disconnects at the necks, and a broad size distribution of fragments results. When clusters containing oxygen impinge on the primary fractal, local melting occurs, leaving the impurities as surface atoms. As it has been reported the oxygen then strongly accelerates the mobility of the neighboring silver atoms, possibly via Ag_2O entities [15–17]. A characteristic diffusion length much larger than the roughness would generate the formation of a liquidlike surface film, a situation favorable to Rayleigh instability to develop. This leads to the rapid formation of a quasimonodisperse and equally separated drop chains, as observed.

In summary, fractal morphology is a very useful tool to study the mechanisms underlying the relaxation of nonequilibrium shapes. We experimentally found that the morphological changes of fractal islands formed through the deposition of silver clusters on graphite after increasing surface self-diffusion may present quite different behaviors depending on the nature of the excess energy that activates the relaxation. Since both processes obey hydrodynamics equations, the origin of these quite different behaviors should be found in the very early stage of the dynamics.

[1] D'Arcy Thomspson, *On the Growth and Form* (Cambridge University Press, Cambridge, England, 1961).
[2] J. S. Langer, Rev. Mod. Phys. **52**, 1 (1980).
[3] W. W. Mullins and R. F. Sekerka, J. Appl. Phys. **34**, 323 (1963).
[4] J. W. S. Rayleigh, Proc. London Math. Soc. **10**, 4 (1879).
[5] H. Y. Peng, N. Wang, W. S. Shi, Y. F. Zhang, C. S. Lee, and S. T. Lee, J. Appl. Phys. **89**, 727 (2001).
[6] M. E. Toimil Molares, A. G. Balogh, T. W. Cornelius, R. Neumann, and C. Trautmann, Appl. Phys. Lett. **85**, 5337 (2004).
[7] C. Bréchignac, Ph. Cahuzac, F. Carlier, C. Colliex, J. Le Roux, A. Masson, B. Yoon, and Uzi Landman, Phys. Rev. Lett. **88**, 196103 (2002).
[8] R. Q. Hwang, J. Schröder, C. Günther, and R. J. Behm, Phys. Rev. Lett. **67**, 3279 (1991).
[9] E. Sharon, M. G. Moore, W. D. McCormick, and H. L. Swinney, Phys. Rev. Lett. **91**, 205504 (2003).
[10] R. Sempéré, D. Bourret, T. Woignier, J. Phalippou, and R. Jullien, Phys. Rev. Lett. **71**, 3307 (1993).
[11] T. Irisawa, M. Uwaha, and Y. Saito, Europhys. Lett. **30**, 139 (1995).
[12] M. Conti, B. Meerson, and P. V. Sasorov, Phys. Rev. Lett. **80**, 4693 (1998).
[13] M. Conti, A. Lipshtat, and B. Meerson, Phys. Rev. E **69**, 031406 (2004).
[14] R. Thouy, N. Olivi-Tran, and R. Julien, Phys. Rev. B **56**, 5321 (1997).
[15] Xiofeng Lai, T. P. St. Clair, and D. W. Goodman, Faraday Discuss. **114**, 279 (1999).
[16] A. R. Layson and P. A. Thiel, Surf. Sci. **472**, L151 (2001).
[17] A. R. Layson, J. W. Evans, and P. A. Thiel, Phys. Rev. B **65**, 193409 (2002).
[18] B. Yoon, V. M. Akulin, Ph. Cahuzac, F. Carlier, M. de Frutos, A. Masson, C. Mory, C. Colliex, and C. Bréchignac, Surf. Sci. **443**, 76 (1999).
[19] T. A. Witten and L. M. Sander, Phys. Rev. Lett. **47**, 1400 (1981).